
Language Reconstruction with Brain Predictive Coding from fMRI Data

Congchi Yin^{1,2} Ziyi Ye³ Piji Li^{1,2*}

¹Nanjing University of Aeronautics and Astronautics

²MIT Key Laboratory of Pattern Analysis and Machine Intelligence, Nanjing, China

³Tsinghua University, Beijing, China

{congchiyin,pjli}@nuaa.edu.cn yeziyi1998@gmail.com

Abstract

Many recent studies have shown that the perception of speech can be decoded from brain signals and subsequently reconstructed as continuous language. However, there is a lack of neurological basis for how the semantic information embedded within brain signals can be used more effectively to guide language reconstruction. The theory of predictive coding suggests that human brain naturally engages in continuously predicting future word representations that span multiple timescales. This implies that the decoding of brain signals could potentially be associated with a predictable future. To explore the predictive coding theory within the context of language reconstruction, this paper proposes a novel model PREDFT for jointly modeling neural decoding and brain prediction. It consists of a main decoding network for language reconstruction and a side network for predictive coding. The side network obtains brain predictive coding representation from related brain regions of interest with a multi-head self-attention module. This representation is fused into the main decoding network with cross-attention to facilitate the language models' generation process. Experiments are conducted on the largest naturalistic language comprehension fMRI dataset Narratives. PREDFT achieves current state-of-the-art decoding performance with a maximum BLEU-1 score of 27.8%.

1 Introduction

Reconstructing natural language from functional magnetic resonance imaging (fMRI) signals offers potential insights into understanding the formation of language in the human brain. Recent studies have attempted to leverage brain signals with computational language models to generate coherent, naturally flowing languages [3, 37, 1, 44]. This advancement is achieved based on the ability of computational language models to craft coherent language, with brain responses serving as guidance in the generation process, thereby aligning the model's output with human perception. For example, Tang et al. [33] used a GPT [27] model to generate semantic candidates, and then brain signals are employed to select the content that is more aligned with the semantic content perceived by humans. Xi et al. [41] proposed to fuse the brain representation as the input for language model and achieves language reconstruction through sequence-to-sequence machine translation [32].

Despite relatively good decoding quality, existing works often overlook how the natural language is encoded within human brain as well as its representation within language models, which is significant for understanding the language reconstruction process. *Predictive coding* [20, 29, 9] provides an attractive theory for a unified view of neural encoding and decoding. It suggests that human brain naturally makes predictions of future words over multiple timescales when receiving current phonetic

*Corresponding author.

stimuli. Previous neuroscience studies [39, 24] have already evidenced such speech prediction in human brain through fMRI. Caucheteux et al. [5] further investigated the correlation between language model representation and brain predictive coding. After confirming the activations of modern language models could be linearly mapped to brain responses, they demonstrated that such brain mapping would be enhanced by adding predictive content to language model input. These findings in neural encoding remind us that in the language reconstruction process, treating brain signals as inputs without considering temporal relationships related to the predictive process may not be sufficient. However, whether brain predictive coding could really help facilitate fMRI-to-text decoding and how to exploit the prediction in decoding still remain unexplored.

To investigate predictive coding from the perspective of decoding, we first conduct a preliminary experiment to analyze the capability of brain signals in predicting future content and their associative relationship with the representations of language models. We verify the predictive coding ability of brain signals and identify six brain regions of interests that are most related to the predictive coding functions. Based on the observations, we propose PREDFT, abbreviation of **F**MRI-to-**T**ext decoding with **P**redictive coding, for jointly modeling language reconstruction and brain predictive coding. PREDFT is an end-to-end model with a main decoding network for language reconstruction and a side network for providing brain predictive coding heuristics. The main decoding network consists of an encoding model for spatial-temporal feature extraction and a Transformer [35] variant for generation. The encoding model applies a 3D convolutional neural network [14] to extract spatial features of fMRI and a finite impulse response model [13] to compensate for the delay of blood-oxygen-level-dependent signal. At the same time, the side network extracts and fuses six regions of interest related to brain predictive coding, and then builds mappings with the main decoding network through cross-attention mechanism.

Experiments are conducted on a large naturalistic language comprehension fMRI dataset Narratives [23]. First, we present the overall decoding performance of PREDFT. We show that its decoding performance outperforms existing proposed methods in terms of a series of language similarity metrics. Second, we explore whether the selection of regions of interest for the side network will affect the decoding performance of PREDFT. This experiment aims to confirm that the brain predictive coding functions only originate in certain spatial regions from decoding perspective. Last, we analyze the distance in predictive coding to better understand how the human brain makes predictions over multiple timescales and its influence on language reconstruction performance.

The main contributions of this paper can be summarized as follows: (i) To the best of our knowledge, we first investigate the brain predictive coding issue from the perspective of decoding brain signals into natural language. (ii) We propose an end-to-end model PREDFT for fMRI-to-text decoding, which features effectively utilizing brain predictive coding representation to improve decoding performance through a side network. (iii) Experimental results show that PREDFT benefits from the joint modeling of brain predictive coding and achieves state-of-the-art decoding performance.

2 Predictive Coding Verification

In this section, we elaborate on predictive coding in human brain by analyzing the correlation between brain responses stimulated by spoken words and activations of language model with the spoken words as input. Following previous study [4], the brain score $R(\mathbf{X}) = \text{corr}(f(\mathbf{X}), \mathbf{Y})$ is first defined, which measures the pearson correlation between language model activations $\mathbf{X} \in \mathbb{R}^{M \times D}$ and brain responses $\mathbf{Y} \in \mathbb{R}^{N \times V}$, where f is a linear ridge regression model with ℓ_2 -regularization for linear mapping. M and N stand for the number of words and fMRI frames; D and V stand for the output dimension of language model and number of voxels in brain. Similar to [5], prediction score $P_{(d,l)}(\mathbf{X}) = R(\mathbf{X} \oplus \mathbf{X}_l^d) - R(\mathbf{X})$ is proposed, which is the difference between brain score of the concatenation of current word with future words and brain score of the current word. \mathbf{X}_l^d indicates the representation of l continuous future heard words with prediction distance d which measures the distance from current word to the last future heard word. Sub-figure (a) of Figure 1 shows an example of \mathbf{X}_2^5 . Prediction score reflects the degree of predictive coding. A positive value suggests long-range prediction helps improve the correlation between language model activations and brain responses. In experiment, the output of eighth layer in GPT-2 [28] is applied for \mathbf{X} . The brain score is averaged across subjects and computed within one fMRI frame, namely N is set as 1. The prediction score is calculated with fixed window length $l = 2$ and distance d ranging from 0 to 11.

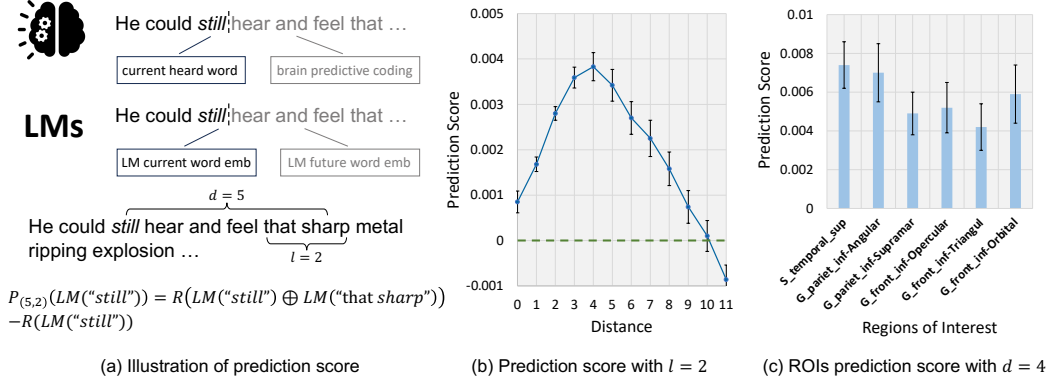


Figure 1: Example and results of the predictive coding verification experiment.

The sub-figure (b) in Figure 1 reports the prediction score across individuals with 95% confidence intervals. Results show prediction score $P_{(d,l)}(\mathbf{X})$ first increases and peaks at $d = 4$, then decreases as the prediction distance d increases, and finally goes down below zero when the prediction distance comes to $d = 10$. We also conduct regions of interest (ROI) analysis. Six regions related to brain predictive coding, including superior temporal sulcus, angular gyrus, supramarginal gyrus, and opercular, triangular, and orbital part of the inferior frontal gyrus in the left hemisphere, are selected for experiments. Sub-figure (c) shows the prediction score of six ROIs across individuals with 95% confidence intervals. The prediction distance is set at $d = 4$ for the best predictive performance, as reflected in sub-figure (b). All the selected ROIs show positive response to prediction words.

The above verification experiment highlights the correlation between language model representation and brain predictive coding. One possible explanation for the phenomenon is that both language models and brain predictive coding are similar in the objective of upcoming words prediction. This inspires us with the following motivation: While predictive coding has been verified from the perspective of encoding, could it help in decoding brain signals into natural language with autoregressive generation? We propose PREDFT for investigating the effectiveness of utilizing brain prediction in fMRI-to-text decoding. Details are introduced in the next section.

3 Methodology

We first formalize the fMRI-to-text decoding task. Given a naturalistic language comprehension fMRI dataset $\mathcal{D} := \{F_{ij}, U_j\}$, where U_j is j -th fragment of word stimuli and F_{ij} is the fMRI data collected while the i -th subject is hearing the content of U_j . The fMRI-to-text decoding task aims to build a model \mathcal{M} that decodes $U'_j = \mathcal{M}(F_{ij})$ to maximize the similarity between U_j and U'_j , which is measured by a text similarity metric D . Specifically, the word stimuli segment $U_j = \{u_j^T, u_j^{T+1}, \dots, u_j^{T+k}\}$ is the auditory content presented to the subject from time step T , where each u_j^T contains a series of corresponding word tokens. Similarly, $F_{ij} := \{f_{i,j}^T, f_{i,j}^{T+1}, \dots, f_{i,j}^{T+k}\}$ consists of $k+1$ continuous fMRI images starting from time step T . Each u_j matches $f_{i,j}$ at corresponding time step t .

We propose PREDFT, which integrates brain predictive coding function in the language reconstruction process. PREDFT is denoted as $\mathcal{M}_{\theta,\phi}$, containing a main decoding network \mathcal{M}_{θ} and a side network \mathcal{M}_{ϕ} for brain predictive coding. We first introduce the main decoding network \mathcal{M}_{θ} which can reconstruct accurate text from fMRI with computational language models. Then we elaborate on the side network \mathcal{M}_{ϕ} which extracts and exploits brain predictive coding. Finally, the fusion of brain predictive coding representation and the joint training of \mathcal{M}_{θ} and \mathcal{M}_{ϕ} are introduced.

3.1 Main Decoding Network

As shown in Figure 2, the main decoding network \mathcal{M}_{θ} consists of an encoder $\mathcal{M}_{\theta_{\text{Enc}}}$ and a decoder $\mathcal{M}_{\theta_{\text{Dec}}}$. The encoder $\mathcal{M}_{\theta_{\text{Enc}}}$ is stacked with a 3D-CNN module, a finite impulse response (FIR) model [13], and a Transformer encoder [35]. For each fMRI image $f_{i,j}^T \in \mathbb{R}^{w \times h \times d}$, where w, h, d

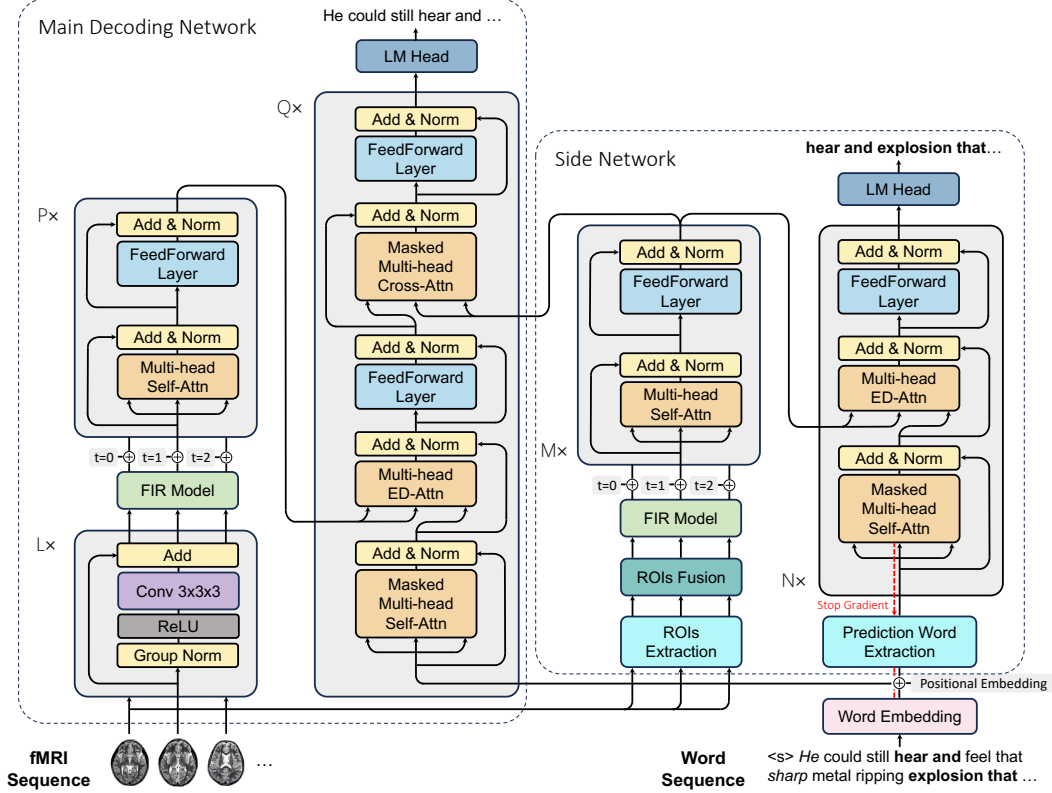


Figure 2: The general framework of PREDFT. The italic type words in the input word sequence stand for the first heard word of each fMRI image while the bold words stand for the prediction words.

represents the width, height, and depth, voxel-level normalization is first applied. Details are described in Appendix A. The fMRI image after normalization is denoted as $\hat{f}_{i,j}^T$, which is then fed into the 3D-CNN module. The 3D-CNN module contains L layers of group normalization [40], ReLU activation, and convolution layer [16], with residual connection [11]. The size of fMRI image $\hat{f}_{i,j}^T$ is progressively reduced by convolution layer and finally downsized to $\hat{f}_{i,j}^T \in \mathbb{R}^{w' \times h' \times d' \times c}$ where c is the number of output channels. A flatten layer and a linear layer are used to obtain a one-dimensional vector $x_{i,j}^T \in \mathbb{R}^{d_m}$ as the output of the 3D-CNN module. After that, a FIR model g_t is applied to compensate for the latency of blood-oxygen-level-dependent (BOLD) signal. For $k+1$ continuous fMRI images with $t \in \{T, T+1, \dots, T+k\}$, the temporal transformation g_t concatenates $k-k^*$ future frames to form the representation in time step t :

$$g_t : \mathbb{R}^{k \times d_m} \rightarrow \mathbb{R}^{k^* \times (d_m(k-k^*))} \quad (1)$$

$$x_{i,j}^t \mapsto \text{concat}(x_{i,j}^t, x_{i,j}^{t+1}, \dots, x_{i,j}^{t+(k-k^*)}), t \in \{T, T+1, \dots, T+k^*\}.$$

where $k - k^*$ is the number of delays. Then a linear layer $\mathbf{W}_{ll} \in \mathbb{R}^{(d_m(k-k^*)) \times d_m}$ is used to fuse delayed brain responses and recover $x_{i,j}^t$ into its original dimension d_m . After learning the spatial features of fMRI images, the representations with learnable time positional embeddings, denoted as $\mathbf{H}_{\text{Enc}}^0 \in \mathbb{R}^{k^* \times d_m}$, are sent into a Transformer encoder to capture temporal features within given intervals. The output of the Transformer encoder is $\mathbf{H}_{\text{Enc}}^P = \mathcal{M}_{\theta_{\text{Enc}}}(\mathbf{H}_{\text{Enc}}^0)$, where P is the number of Transformer encoder layers.

Finally, the output from $\mathcal{M}_{\theta_{\text{Enc}}}$, i.e., $\mathbf{H}_{\text{Enc}}^P$, is fed into the decoder $\mathcal{M}_{\theta_{\text{Dec}}}$. $\mathcal{M}_{\theta_{\text{Dec}}}$ contains modules within a standard Transformer decoder consisting of masked multi-head self-attention, multi-head encoder-decoder attention, and feed-forward layer. Besides, additional masked multi-head cross-attention layer and feed-forward layer are designed for $\mathcal{M}_{\theta_{\text{Dec}}}$. The cross-attention layer integrates brain predictive coding representations inherited from the side network. More details will be

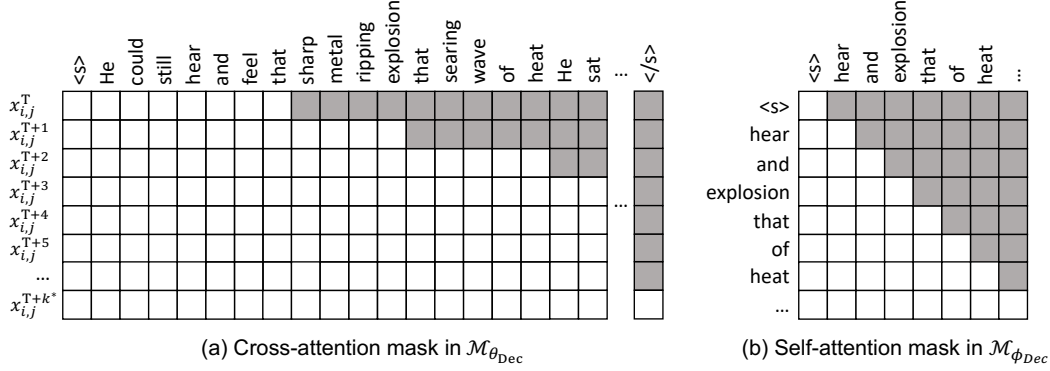


Figure 3: Illustration of attention masks. Grey color indicates mask. The cross-attention mask is transposed for simplicity of expression.

introduced in Section 3.3 and here we just view it as an encoder-decoder attention layer. The shifted right text U_j^r is first tokenized and sent into a word embedding layer \mathbf{W}_{word} to get representations $\mathbf{H}_{\theta_{Dec}}^0$. We denote the input of the $(l+1)$ -th self-attention layer as $\mathbf{H}_{\theta_{Dec}}^l$, so the self-attention is calculated by

$$\text{Self-Attn}(\mathbf{H}_{\theta_{Dec}}^l \mathbf{W}_Q^l, \mathbf{H}_{\theta_{Dec}}^l \mathbf{W}_K^l, \mathbf{H}_{\theta_{Dec}}^l \mathbf{W}_V^l) = \text{softmax}\left(\frac{\mathbf{H}_{\theta_{Dec}}^l \mathbf{W}_Q^l (\mathbf{H}_{\theta_{Dec}}^l \mathbf{W}_K^l)^\top}{\sqrt{d_k}}\right) \mathbf{H}_{\theta_{Dec}}^l \mathbf{W}_V^l, \quad (2)$$

where $\mathbf{W}_Q^l, \mathbf{W}_K^l, \mathbf{W}_V^l \in \mathbb{R}^{d_m \times d_k}$ are the parameter matrices of projecting query, key, value in the $(l+1)$ -th corresponding layer (i.e. here is the self-attention layer) for simplicity. The encoder-decoder attention aims to integrate fMRI representations. It takes $\mathbf{H}_{\theta_{Dec}}^l$ as query and $\mathbf{H}_{\theta_{Enc}}^P$ for key and value:

$$\text{ED-Attn}(\mathbf{H}_{\theta_{Dec}}^l \mathbf{W}_Q^l, \mathbf{H}_{\theta_{Enc}}^P \mathbf{W}_K^l, \mathbf{H}_{\theta_{Enc}}^P \mathbf{W}_V^l) = \text{softmax}\left(\frac{\mathbf{H}_{\theta_{Dec}}^l \mathbf{W}_Q^l (\mathbf{H}_{\theta_{Enc}}^P \mathbf{W}_K^l)^\top}{\sqrt{d_k}}\right) \mathbf{H}_{\theta_{Enc}}^P \mathbf{W}_V^l. \quad (3)$$

The attention masks for self-attention and encoder-decoder attention are the same as vanilla Transformer. The final output of $\mathcal{M}_{\theta_{Dec}}$ is denoted as $\mathbf{H}_{\theta_{Dec}}^Q$ where Q is the number of decoder layers.

3.2 Side Network for Predictive Coding

The idea of designing a side network \mathcal{M}_ϕ for brain predictive coding is motivated by predictive coding theory [20, 29, 9], which indicates the human brain naturally makes predictions about words over multiple timescales. Since brain predictive coding has been verified from the perspective of encoding (the linear mapping between language models and brain responses), we hope to exploit it by training a neural network to well represent regions involved in prediction and fusing brain predictive coding representations in decoding. A vanilla Transformer \mathcal{M}_ϕ with encoder $\mathcal{M}_{\phi_{Enc}}$ and decoder $\mathcal{M}_{\phi_{Dec}}$ is applied for brain predictive coding. Specifically, it takes $R_{ij} := \{r_{i,j}^T, r_{i,j}^{T+1}, \dots, r_{i,j}^{T+k}\}$ as encoder input and $V_j^r := \{\langle s \rangle, v_j^T, v_j^{T+1}, \dots, v_j^{T+k}\}$ as decoder input. As shown in Figure 2, each $r_{i,j}^T \in \mathbb{R}^{d_r}$ in R_{ij} extracted from $f_{i,j}^T$ in F_{ij} is one-dimensional cerebral cortex data. It stands for the concatenation of regions of interest (ROIs) related to brain predictive coding as verified in Section 2. Each v_j^T in V_j^r stands for the l future words with prediction distance d (recall the definition in Section 2) of u_j^T in U_j^r that human brain predicts. The side network \mathcal{M}_ϕ is trained to learn the mapping from brain predictive responses to ground truth future words.

The ROI fusion layer is a fully connected feed-forward network that outputs the representation $r_{i,j}^T \in \mathbb{R}^{d_m}$. The same FIR model in the main decoding network is applied to compensate for the delays of the BOLD signal. Learnable time positional embedding is added to $r_{i,j}^T$ before entering

into the Transformer encoder $\mathcal{M}_{\phi_{\text{Enc}}}$ with M layers. The output of $\mathcal{M}_{\phi_{\text{Enc}}}$ is denoted as $\mathbf{H}_{\phi_{\text{Enc}}}^M$, which stands for the representation of brain predictive coding. $\mathbf{H}_{\phi_{\text{Enc}}}^M$ plays an essential role in PREDFT, as it will be fused into the main decoding network to verify the effectiveness of brain predictive coding in the decoding task. The Transformer decoder $\mathcal{M}_{\phi_{\text{Dec}}}$ follows the conventional practice of masked self-attention and encoder-decoder attention, which has been elaborated in Equation 2 and Equation 3 of Section 3.1, respectively.

3.3 Prediction Fusion and Joint Training

The subsection details how the brain predictive coding representation from the side network fuses into the main decoding network. As shown in Figure 2, the brain predictive coding representation $\mathbf{H}_{\phi_{\text{Enc}}}^M$, which is the output of $\mathcal{M}_{\phi_{\text{Enc}}}$, plays as keys and values for the masked cross-attention in the main decoding network. The queries of cross-attention layer are the output from the previous encoder-decoder attention layer and feed-forward layer. The cross attention is formularized as:

$$\text{Cross-Attn}(\mathbf{H}_{\theta_{\text{Dec}}}^l \mathbf{W}_Q^l, \mathbf{H}_{\phi_{\text{Enc}}}^M \mathbf{W}_K^l, \mathbf{H}_{\phi_{\text{Enc}}}^M \mathbf{W}_V^l) = \text{softmax}\left(\frac{\mathbf{H}_{\theta_{\text{Dec}}}^l \mathbf{W}_Q^l (\mathbf{H}_{\phi_{\text{Enc}}}^M \mathbf{W}_K^l)^\top}{\sqrt{d_k}}\right) \mathbf{H}_{\phi_{\text{Enc}}}^M \mathbf{W}_V^l. \quad (4)$$

The mask $\mathbf{M}_{\text{ca}} \in \mathbb{R}^{k_t \times k^*}$ of cross-attention is shown in Figure 3(a). k_t and k^* are the numbers of input tokens and fMRI signals, respectively. The cross-attention mask \mathbf{M}_{ca} is designed in this way: for each token in the text fragment u_j^t , all the predictive coding representations after time step t are allowed to attend, while previous representations are masked.

PREDFT is trained in an end-to-end manner. The main decoding network \mathcal{M}_θ and the side network \mathcal{M}_ϕ share the same word embedding layer \mathbf{W}_{word} , whose parameters are only updated with the gradient flow from \mathcal{M}_θ during training. The training objective follows a left-to-right auto-regressive language modeling manner for both \mathcal{M}_θ and \mathcal{M}_ϕ . Specifically, following \mathcal{M}_θ and \mathcal{M}_ϕ are two language model heads \mathbf{W}_θ and \mathbf{W}_ϕ . The training loss for \mathcal{M}_θ is

$$\mathcal{L}_{\text{Main}} = - \sum_{t=1}^n \log P(y_t | y_{<t}, U_j^r; \theta), \quad (5)$$

where U_j^r is the input and y_t is the generated token. Similarly, the training loss for \mathcal{M}_ϕ is

$$\mathcal{L}_{\text{Side}} = - \sum_{t=1}^n \log P(z_t | z_{<t}, V_j^r; \phi). \quad (6)$$

The joint training of \mathcal{M}_θ and \mathcal{M}_ϕ is to optimize $\mathcal{L} = \mathcal{L}_{\text{Main}} + \lambda \mathcal{L}_{\text{Side}}$, where λ is a hyper-parameter.

4 Experimental Settings and Results

Several experiments are conducted to (i) evaluate the decoding performance of PREDFT (ii) detailedly analyze how brain predictive coding work in PREDFT. First we briefly introduce the experimental settings, while more details are shown in Appendix A. Then the results of decoding performance, regions of interest selection analysis, and prediction distance analysis are displayed. Besides, we investigate the decoding error distribution of different models in Appendix B and conduct ablation study in Appendix C.

4.1 Baselines and Evaluation Metrics

The decoding performance of PREDFT is compared to current state-of-the-art model UniCoRN [41]. We don't test [33] and [42] in experiments because their model settings aren't compatible with the dataset splitting method or preprocessed version we applied. Details are discussed in Appendix A.

Automatic evaluation metrics including BLEU [25] and ROUGE [19] are applied to measure decoding performance of different models. BLEU measures the n-gram overlap between decoded content and ground truth. ROUGE-N computes the precision, recall, and F1-score based on the n-gram overlap. Specifically, BLEU-1/2/3/4 and ROUGE1-R/P/F are used for all experiments.

Table 1: Performance of different models in fMRI-to-text decoding. Length denotes to the length of continuous fMRI frames.

Length	Model	BLEU-N (%)				ROUGE-1 (%)		
		$N = 1$	$N = 2$	$N = 3$	$N = 4$	R	P	F
10	UniCoRN	20.64	5.03	1.40	0.45	15.56	25.47	19.23
	PREDFT	24.73	8.39	3.92	1.86	14.07	35.28	19.53
20	UniCoRN	18.02	4.71	1.32	0.4	18.01	29.46	20.82
	PREDFT	25.98	5.61	1.36	0.21	19.61	25.43	22.09
40	UniCoRN	21.76	5.43	1.17	0.34	19.76	35.33	25.30
	PREDFT	27.80	8.29	2.00	0.54	19.53	38.95	25.96

Table 2: The decoding performance of PREDFT when different ROIs are selected for the side network. Random means randomly picking ROIs. Whole stands for using whole human cerebral cortex. BPC denotes to the ROIs related to brain predictive coding.

Length	ROIs Selection	BLEU-N (%)				ROUGE-1 (%)		
		$N = 1$	$N = 2$	$N = 3$	$N = 4$	R	P	F
10	None	18.08	3.98	1.05	0.28	14.96	26.21	18.96
	Random	16.83	3.04	0.63	0.13	16.71	19.23	17.28
	Whole	21.99	4.51	0.83	0.25	17.36	22.83	19.43
	BPC	24.73	8.39	3.92	1.86	14.07	35.28	19.53
20	None	20.37	3.86	1.03	0.19	17.42	22.15	19.45
	Random	16.11	3.28	0.55	0.12	19.27	24.29	21.44
	Whole	23.55	6.39	1.33	0.39	15.66	30.98	20.72
	BPC	25.98	5.61	1.36	0.21	19.61	25.43	22.09
40	None	18.01	4.72	1.27	0.34	16.41	34.36	22.16
	Random	19.71	5.01	1.22	0.39	20.02	29.61	24.55
	Whole	24.67	5.81	1.14	0.39	20.53	29.46	24.16
	BPC	27.80	8.29	2.00	0.54	19.53	38.95	25.96

4.2 Decoding Performance

We compare the decoding performance of different models on automatic evaluation metrics. To further investigate the effect of fMRI sequence length on decoding model performance, experiments are separately conducted with fMRI sequence length of 10, 20, and 40, which equals to 15s, 30s, and 60s of fMRI with 1.5s TR. To the best of our knowledge, we are the first to try decoding one-minute of fMRI data. Results are shown in Table 1. Despite UniCoRN’s good performance in some evaluation index like ROUGE1-R, PREDFT achieves the best overall performance on all three experiments with different fMRI sequence lengths. Specifically, it gets the highest BLEU-1 score of 27.8% on decoding 40 continuous fMRI frames. From the relative low results of BLEU-2/3/4, we find all the models struggle to generate long accurate text. It’s still a challenging task to decode fMRI to text. Furthermore, we don’t find clear evidence indicating that the fMRI sequence length has an impact on the performance of the decoding models from experiments.

4.3 Regions of Interest Selection

To better understand whether PREDFT benefits from introducing brain predictive coding, we select different regions of interest (ROIs) for the side network to test their influence on decoding performance. Results are listed in Table 2. Specifically, four types of ROIs are selected: (a) “None” indicates no ROIs are chosen. The side network together with the cross-attention layer in the main decoding network is detached from PREDFT under this setting. (b) “Random” means we randomly pick six ROIs apart from brain predictive coding regions. Specifically, G_and_S_cingul-Ant, G_and_S_subcentral, G_and_S_transv_frontopol, G_orbital, S_front_middle, S_subparietal are chosen in experiment. (c)

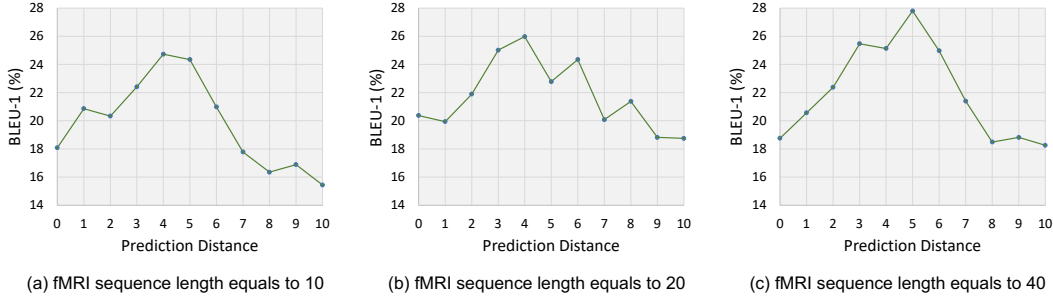


Figure 4: The influence of prediction distance to decoding performance.

Table 3: Two cases of decoded content. Bold type words indicate key concepts or phrases.

Case1	Truth: It was more real than any dream he had ever had in his life. He could still hear and feel that sharp metal ripping explosion that searing wave of heat. He sat
	UniCoRN: It’s than I just a said of a a the hand. You have I the the the you I I I in to at the to to sit .
	PREDFT: It’s a more than normal just good dream about to said. He open the eyes I have be her I like she and and and he and of under the next and I look the platform
Case2	Truth: He couldn’t shake the thought out of his mind. It persisted all through the day until dinner . He was still brooding as he and Mary got ready for bed . Guy dear . Hm oh no. Anything wrong
	UniCoRN: And I know a Dean and a eyes it. And of the first and the and a to guy him. I said I to to him out and And to in that in the end.
	PREDFT: He don’t know my girl you of the eyes but his girl sleep he and he said and he said and the to the and and which I not wrong . But the Guy

“Whole” means the whole human cerebral cortex (74 ROIs in the used atlas, see Appendix A) is applied for brain prediction. (d) “BPC” denotes to the six ROIs related to brain predictive coding as verified in Section 2. BPC leads to the best performance while whole ROIs selection also performs well. However, both random selection and non-selection lead to poor decoding accuracy, and random selection causes worse performance in most cases. Two conclusions could be drawn from the above ROIs analysis. First, the predictive coding information only contains in specific regions of human brain. Second, brain predictive coding can be beneficial to decoding models with proper network architecture design (e.g. PREDFT).

4.4 Prediction Distance Analysis

In this section, we investigate the influence of prediction distance to the decoding performance of PREDFT. Experiments are conducted with a fixed window length $l = 2$ and the influence of prediction distance is reflected through BLEU-1 score. Figure 4 shows the results with different fMRI sequence lengths. We notice a similar phenomenon as the predictive coding verification experiment in Section 2. The trend of BLEU-1 score first rises then falls as prediction distance d increases. PREDFT achieves the best performance with prediction distance around four. The prediction distance analysis highlights two findings: (i) The design of a side network in PREDFT successfully fuses brain prediction for decoding. (ii) The influence of prediction distance in fMRI-to-text decoding is consistent with that in linearly mapping language models to brain response.

4.5 Case Study

Some fMRI-to-text decoding cases with fMRI sequence length equals to 10 are listed in Table 3. From the cases, we find PREDFT successfully decodes some high-level semantic concepts and key words compared to UniCoRN. For example, in case1 PREDFT conveys the meaning of “the best dream” while UniCoRN fails to. In case2, PREDFT decodes the meaning of “he and Mary prepare to sleep”.

Overall, PREDFT performs better than UniCoRN. However, despite the relative good automatic evaluation performance, all models struggle to decode generally accurate content, especially in (i) generating fluent and coherent sentences (ii) capturing fine-grained semantic meanings (iii) decoding terminology (e.g. name “Mary”) or complicated phrases (e.g. “sharp metal ripping explosion”).

5 Related Work

fMRI-to-Text Decoding. Previous studies focused on aligning fMRI signal to a limited vocabulary of hundred tokens and performing word-level decoding [3, 37, 1, 44], or incorporating fMRI representation into sentence embedding and applying pairwise classification for sentence-level generation [26, 31]. Recently, researchers turned to powerful pretrained language models for open-vocabulary fMRI-to-text decoding. Tang et al. [33] designed a pipeline model where the encoder is responsible for identifying the most possible word sequence among candidates generated by GPT-2 model with beam search. Xi et al. [41] proposed a three-phase training framework UniCoRN which applies BART [17] model for generation. Ye et al. [42] proposed BrainLLM by concatenating fMRI embedding with word embedding as input prompt to fine-tune a Llama2 [34] model.

Brain Predictive Coding. Predictive coding theory [20, 29, 9] aims to propose a potential unifying theory for computational and cognitive neuroscience [21]. It was initially proposed as a neuroscientific theory [22] and subsequently developed into its mathematical form of cortical responses [8]. Although originally formulated to investigate brain visual processing, it was also extended to language processing in human brain in previous work [10, 36]. Predictive coding suggests that human brain naturally makes predictions about future words and sentences when it perceives natural language stimuli. Such hypothesis has already been evidenced by correlating word or phonetic surprisal with fMRI or EEG [39, 24, 7, 12]. Caucheteux et al. [5] further proved a predictive coding hierarchy in the human brain listening to speech by investigating the linear mapping between modern language models and brain responses.

6 Discussion

In this presented study, we focus on brain predictive coding theory and neural decoding. Specifically, we step further on the basis of current predictive coding theory by investigating its effectiveness in decoding fMRI signals into natural language. Predictive coding is first verified by linearly mapping the activations of current auto-regressive language model to brain responses. Then fMRI-to-text decoding model PREDFT is proposed, which features utilizing a side network to capture and fuse brain prediction. Comprehensive experiments demonstrate the good decoding performance of PREDFT benefits from integrating brain predictive coding.

While lots of studies have confirmed the representations drawn from auto-regressive language models are effective at predicting brain responses stimulated by hearing spoken words, the reasons behind such phenomenon are still controversial. A possible convincing explanation is both of the language models and human brain follow a next words prediction pattern. But Antonello and Huth [2] questioned this hypothesis and claimed the language models are effective at predicting brain responses because they generally capture a wide variety of linguistic phenomena. In this paper, we don’t seek to find a proper explanation but try to investigate predictive coding from the perspective of decoding. This finding offers a novel view for future research in predictive coding.

Neural decoding is another popular research topic. Thanks to the development of deep learning, decoding non-invasive signals is becoming possible. However, despite the improvement in decoding performance in PREDFT, we find it’s still extremely difficult to reconstruct natural language from fMRI signals during experiments. The reasons can be summarized as follows: First, the noise inherited from collecting fMRI data is a natural barrier to decoding. Second, different from fMRI-to-image decoding [38, 30] whose experimental setting is letting subjects look at pictures one by one with certain intervals, the fast spoken word rate isn’t compatible with the poor temporal resolution of fMRI data in fMRI-to-text decoding. So part of the brain responses are not recorded in fMRI. Such hypothesis has been evidenced through experiments in Appendix B. Building a dataset with high-resolution devices (e.g. 7T MRI scanner) will probably alleviate this problem.

The limitations of this work include: (i) Experiments are only conducted on Narratives. It's better to try other datasets like [15] or [26]. (ii) We apply cross-subject dataset splitting for all experiments. It's better to supplement experiments on per-subject splitting to get more comprehensive comparisons. (iii) The window length of future words is set as $l = 2$ in experiments due to the limited computational resources. We leave the exploration of future words window length to future work. (iv) Surprising content might become distraction in brain predictive coding. We leave it as future work to analyze.

Acknowledgements

This research is supported by the National Natural Science Foundation of China (No.62106105), the CCF-Baidu Open Fund (No.CCF-Baidu202307), the CCF-Zhipu AI Large Model Fund (No.CCF-Zhipu202315), the Scientific Research Starting Foundation of Nanjing University of Aeronautics and Astronautics (No.YQR21022), and the High Performance Computing Platform of Nanjing University of Aeronautics and Astronautics.

References

- [1] Nicolas Affolter, Beni Egressy, Damian Pascual, and Roger Wattenhofer. Brain2word: decoding brain activity for language generation. *arXiv preprint arXiv:2009.04765*, 2020.
- [2] Richard Antonello and Alexander Huth. Predictive coding or just feature discovery? an alternative account of why language models fit brain data. *Neurobiology of Language*, 5(1): 64–79, 2024.
- [3] Shohini Bhattachali, Murielle Fabre, Wen-Ming Luh, Hazem Al Saied, Mathieu Constant, Christophe Pallier, Jonathan R Brennan, R Nathan Spreng, and John Hale. Localising memory retrieval and syntactic composition: an fmri study of naturalistic language comprehension. *Language, Cognition and Neuroscience*, 34(4):491–510, 2019.
- [4] Charlotte Caucheteux, Alexandre Gramfort, and Jean-Rémi King. Deep language algorithms predict semantic comprehension from brain activity. *Scientific reports*, 12(1):16327, 2022.
- [5] Charlotte Caucheteux, Alexandre Gramfort, and Jean-Rémi King. Evidence of a predictive coding hierarchy in the human brain listening to speech. *Nature human behaviour*, 7(3):430–441, 2023.
- [6] Christophe Destrieux, Bruce Fischl, Anders Dale, and Eric Halgren. Automatic parcellation of human cortical gyri and sulci using standard anatomical nomenclature. *NeuroImage*, 53(1): 1–15, 2010. ISSN 1053-8119. doi: <https://doi.org/10.1016/j.neuroimage.2010.06.010>. URL <https://www.sciencedirect.com/science/article/pii/S1053811910008542>.
- [7] Peter W Donhauser and Sylvain Baillet. Two distinct neural timescales for predictive speech processing. *Neuron*, 105(2):385–393, 2020.
- [8] Karl Friston. Hierarchical models in the brain. *PLoS computational biology*, 4(11):e1000211, 2008.
- [9] Karl Friston and Stefan Kiebel. Predictive coding under the free-energy principle. *Philosophical transactions of the Royal Society B: Biological sciences*, 364(1521):1211–1221, 2009.
- [10] Marta I Garrido, James M Kilner, Klaas E Stephan, and Karl J Friston. The mismatch negativity: a review of underlying mechanisms. *Clinical neurophysiology*, 120(3):453–463, 2009.
- [11] Kaiming He, Xiangyu Zhang, Shaoqing Ren, and Jian Sun. Deep residual learning for image recognition. In *Proceedings of the IEEE conference on computer vision and pattern recognition*, pages 770–778, 2016.
- [12] Micha Heilbron, Kristijan Armeni, Jan-Mathijs Schoffelen, Peter Hagoort, and Floris P De Lange. A hierarchy of linguistic predictions during natural language comprehension. *Proceedings of the National Academy of Sciences*, 119(32):e2201968119, 2022.

- [13] Alexander G Huth, Wendy A De Heer, Thomas L Griffiths, Frédéric E Theunissen, and Jack L Gallant. Natural speech reveals the semantic maps that tile human cerebral cortex. *Nature*, 532 (7600):453–458, 2016.
- [14] Shuiwang Ji, Wei Xu, Ming Yang, and Kai Yu. 3d convolutional neural networks for human action recognition. *IEEE Trans. Pattern Anal. Mach. Intell.*, 35(1):221–231, 2013. doi: 10.1109/TPAMI.2012.59. URL <https://doi.org/10.1109/TPAMI.2012.59>.
- [15] Amanda LeBel, Lauren Wagner, Shailee Jain, Aneesh Adhikari-Desai, Bhavin Gupta, Allyson Morgenthal, Jerry Tang, Lixiang Xu, and Alexander G Huth. A natural language fmri dataset for voxelwise encoding models. *Scientific Data*, 10(1):555, 2023.
- [16] Yann LeCun, Yoshua Bengio, et al. Convolutional networks for images, speech, and time series.
- [17] Mike Lewis, Yinhan Liu, Naman Goyal, Marjan Ghazvininejad, Abdelrahman Mohamed, Omer Levy, Veselin Stoyanov, and Luke Zettlemoyer. BART: Denoising sequence-to-sequence pre-training for natural language generation, translation, and comprehension. In Dan Jurafsky, Joyce Chai, Natalie Schluter, and Joel Tetreault, editors, *Proceedings of the 58th Annual Meeting of the Association for Computational Linguistics*, pages 7871–7880, Online, July 2020. Association for Computational Linguistics. doi: 10.18653/v1/2020.acl-main.703. URL <https://aclanthology.org/2020.acl-main.703>.
- [18] Chien Heng Liao, Keith J Worsley, J-B Poline, John AD Aston, Gary H Duncan, and Alan C Evans. Estimating the delay of the fmri response. *NeuroImage*, 16(3):593–606, 2002.
- [19] Chin-Yew Lin. Rouge: A package for automatic evaluation of summaries. In *Text summarization branches out*, pages 74–81, 2004.
- [20] James L McClelland and David E Rumelhart. An interactive activation model of context effects in letter perception: I. an account of basic findings. *Psychological review*, 88(5):375, 1981.
- [21] Beren Millidge, Anil Seth, and Christopher L Buckley. Predictive coding: a theoretical and experimental review, 2022.
- [22] David Mumford. On the computational architecture of the neocortex: I. the role of the thalamo-cortical loop. *Biological cybernetics*, 65(2):135–145, 1991.
- [23] Samuel A Nastase, Yun-Fei Liu, Hanna Hillman, Asieh Zadbood, Liat Hasenfratz, Neggin Keshavarzian, Janice Chen, Christopher J Honey, Yaara Yeshurun, Mor Regev, et al. The “narratives” fmri dataset for evaluating models of naturalistic language comprehension. *Scientific data*, 8(1):250, 2021.
- [24] Kayoko Okada, William Matchin, and Gregory Hickok. Neural evidence for predictive coding in auditory cortex during speech production. *Psychonomic bulletin & review*, 25:423–430, 2018.
- [25] Kishore Papineni, Salim Roukos, Todd Ward, and Wei-Jing Zhu. Bleu: a method for automatic evaluation of machine translation. In *Proceedings of the 40th annual meeting of the Association for Computational Linguistics*, pages 311–318, 2002.
- [26] Francisco Pereira, Bin Lou, Brianna Pritchett, Samuel Ritter, Samuel J Gershman, Nancy Kanwisher, Matthew Botvinick, and Evelina Fedorenko. Toward a universal decoder of linguistic meaning from brain activation. *Nature communications*, 9(1):963, 2018.
- [27] Alec Radford, Karthik Narasimhan, Tim Salimans, Ilya Sutskever, et al. Improving language understanding by generative pre-training. 2018.
- [28] Alec Radford, Jeffrey Wu, Rewon Child, David Luan, Dario Amodei, Ilya Sutskever, et al. Language models are unsupervised multitask learners. *OpenAI blog*, 1(8):9, 2019.
- [29] Rajesh PN Rao and Dana H Ballard. Predictive coding in the visual cortex: a functional interpretation of some extra-classical receptive-field effects. *Nature neuroscience*, 2(1):79–87, 1999.

- [30] Paul Scotti, Atmadeep Banerjee, Jimmie Goode, Stepan Shabalin, Alex Nguyen, Aidan Dempster, Nathalie Verlinde, Elad Yundler, David Weisberg, Kenneth Norman, et al. Reconstructing the mind’s eye: fmri-to-image with contrastive learning and diffusion priors. *Advances in Neural Information Processing Systems*, 36, 2024.
- [31] Jingyuan Sun, Shaonan Wang, Jiajun Zhang, and Chengqing Zong. Towards sentence-level brain decoding with distributed representations. *Proceedings of the AAAI Conference on Artificial Intelligence*, 33(01):7047–7054, Jul. 2019. doi: 10.1609/aaai.v33i01.33017047. URL <https://ojs.aaai.org/index.php/AAAI/article/view/4685>.
- [32] Ilya Sutskever, Oriol Vinyals, and Quoc V. Le. Sequence to sequence learning with neural networks. In Zoubin Ghahramani, Max Welling, Corinna Cortes, Neil D. Lawrence, and Kilian Q. Weinberger, editors, *Advances in Neural Information Processing Systems 27: Annual Conference on Neural Information Processing Systems 2014, December 8-13 2014, Montreal, Quebec, Canada*, pages 3104–3112, 2014. URL <https://proceedings.neurips.cc/paper/2014/hash/a14ac55a4f27472c5d894ec1c3c743d2-Abstract.html>.
- [33] Jerry Tang, Amanda LeBel, Shailee Jain, and Alexander G Huth. Semantic reconstruction of continuous language from non-invasive brain recordings. *Nature Neuroscience*, 26(5):858–866, 2023.
- [34] Hugo Touvron, Louis Martin, Kevin Stone, Peter Albert, Amjad Almahairi, Yasmine Babaei, Nikolay Bashlykov, Soumya Batra, Prajjwal Bhargava, Shruti Bhosale, et al. Llama 2: Open foundation and fine-tuned chat models. *arXiv preprint arXiv:2307.09288*, 2023.
- [35] Ashish Vaswani, Noam Shazeer, Niki Parmar, Jakob Uszkoreit, Llion Jones, Aidan N Gomez, Łukasz Kaiser, and Illia Polosukhin. Attention is all you need. *Advances in neural information processing systems*, 30, 2017.
- [36] Catherine Wacogne, Etienne Labyt, Virginie Van Wassenhove, Tristan Bekinschtein, Lionel Naccache, and Stanislas Dehaene. Evidence for a hierarchy of predictions and prediction errors in human cortex. *Proceedings of the National Academy of Sciences*, 108(51):20754–20759, 2011.
- [37] Shaonan Wang, Jiajun Zhang, Haiyan Wang, Nan Lin, and Chengqing Zong. Fine-grained neural decoding with distributed word representations. *Information Sciences*, 507:256–272, 2020.
- [38] Shizun Wang, Songhua Liu, Zhenxiong Tan, and Xinchao Wang. Mindbridge: A cross-subject brain decoding framework. *arXiv preprint arXiv:2404.07850*, 2024.
- [39] Roel M Willems, Stefan L Frank, Annabel D Nijhof, Peter Hagoort, and Antal Van den Bosch. Prediction during natural language comprehension. *Cerebral cortex*, 26(6):2506–2516, 2016.
- [40] Yuxin Wu and Kaiming He. Group normalization. In *Proceedings of the European conference on computer vision (ECCV)*, pages 3–19, 2018.
- [41] Nuwa Xi, Sendong Zhao, Haochun Wang, Chi Liu, Bing Qin, and Ting Liu. UniCoRN: Unified cognitive signal Reconstruction bridging cognitive signals and human language. In Anna Rogers, Jordan Boyd-Graber, and Naoaki Okazaki, editors, *Proceedings of the 61st Annual Meeting of the Association for Computational Linguistics (Volume 1: Long Papers)*, pages 13277–13291, Toronto, Canada, July 2023. Association for Computational Linguistics. doi: 10.18653/v1/2023.acl-long.741. URL <https://aclanthology.org/2023.acl-long.741>.
- [42] Ziyi Ye, Qingyao Ai, Yiqun Liu, Min Zhang, Christina Lioma, and Tuukka Ruotsalo. Language generation from human brain activities. *arXiv preprint arXiv:2311.09889*, 2023.
- [43] Congchi Yin, Qian Yu, Zhiwei Fang, Jie He, Changping Peng, Zhangang Lin, Jingping Shao, and Piji Li. Data contamination issues in brain-to-text decoding. *arXiv preprint arXiv:2312.10987*, 2023.
- [44] Shuxian Zou, Shaonan Wang, Jiajun Zhang, and Chengqing Zong. Towards brain-to-text generation: Neural decoding with pre-trained encoder-decoder models. In *NeurIPS 2021 AI for Science Workshop*, 2021.

A Experimental Settings

Dataset and Splitting Method All experiments are conducted on the largest naturalistic language comprehension fMRI dataset Narratives [23], which contains recordings from 345 subjects listening to 27 diverse stories. Since the data collection process involves different machines, only fMRI data with $64 \times 64 \times 27$ voxels is considered, which results to 230 subjects. For the dataset preprocess method, we choose the fMRIPrep version. Xi et al. [41] also applied fMRIPrep while Ye et al. [42] applied the AFNI-smooth version.

How to split datasets for training and evaluation is a matter of debate in fMRI-to-text decoding [41]. Ye et al. [42] and Tang et al. [33] trained and evaluated models per subject. Xi et al. [41] applied cross-subject splitting but has been identified to have data leakage issue [43]. To avoid data leakage and test model’s cross-subject generalization ability, we apply the splitting method proposed in [43].

Implementation Details The latest version of Destrieux atlas [6] is applied for cortical parcellation, which leads to 74 regions per hemisphere. We use six regions of interests that have been proven in [5] to contribute to brain prediction, including superior temporal sulcus, angular gyrus, supramarginal gyrus, and opercular, triangular, orbital part of the inferior frontal gyrus.

Voxel-level normalization is performed to raw fMRI data, which separately normalizes the values of each voxel over the time domain. This normalization highlights the relative activation of a specific voxel within given intervals. In the main decoding network, the numbers of Transformer encoders and decoders are set to $P=4$ and $Q=12$ respectively. For the side network, both are set as $M=N=6$. We apply the tokenizer in BART[17] for our model. PREDFT is trained over 20 epochs with an initial learning rate of $5e-4$ which eventually decays to $1e-5$. The hyper-parameter λ for jointly training the main and side networks is set to 1 for fMRI sequence of length 10, and 0.5 for sequence of length 20 and 40. For baseline methods we strictly follow the settings in the proposed paper [41]. All experiments are conducted on NVIDIA A100-80G GPUs.

B Decoding Error Analysis

In this section, we design an experiment that analyzes the positional distribution of incorrectly decoded words. Figure 5 is an example of two successive fMRI frames containing seven and four spoken words respectively. Three kinds of errors during decoding are defined: (i) The decoding model \mathcal{M} fails to generate the correct word (e.g. “could” is incorrectly decoded as “should”). (ii) The decoding model \mathcal{M} generates redundant words (e.g. repetitive “and”). (iii) Corresponding words are missing during decoding (e.g. “sharp metal ripping” is missing in output). Although some of the generated words are semantically consistent with the ground truth, we apply the strict exact match to facilitate automatic evaluation. Three position counting methods for corresponding errors are proposed: (i) If decoded word is wrong, position index of the corresponding truth word is marked as wrong. (ii) If decoded words are redundant, position index of the last matched truth word is marked as wrong. (iii) If decoded words are missing, position indices of all the missing truth words are marked as wrong. Since different fMRI frames contain different numbers of spoken words, the relative positions of incorrect words within each frame, namely the percentage of index (PosPCT), are considered. The error probability of one specific position is the proportion of errors at this position to the total number of errors. Table (a) in Figure 5 illustrates the positional distribution of incorrectly decoded words in the example. The distribution is calculated at ten percentiles from 10% to 100%. As some positions like 10% or 90% are minority in all statistical positions, we also add the error probabilities of the first and last 50% respectively, as shown in table (b).

Such experiment is conducted on UniCoRN and PREDFT. Positional decoding error distribution and sum of error probability are analyzed. Results are shown in Figure 6. We find the error probability of last heard words in TR is significantly higher than words heard at the beginning. However, the error probabilities of decoding the first and last half of text are supposed to be the same in normal cases. This phenomenon leads to the hypothesis that the information of some heard words, especially the last few words in each TR, is lost in fMRI data. It’s caused by the discrete sampling feature of fMRI: Due to the constraints of MRI scanner in strength and speed of switching the magnetic gradients, the fMRI signal is sampled discretely with a fixed time interval called repetition time (TR) in order to achieve the balance between spacial and temporal resolution. The repetition time in fMRI-to-text decoding task is usually around two seconds. However, the average speaking rate

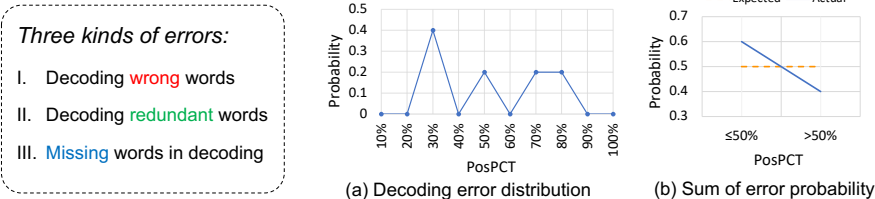
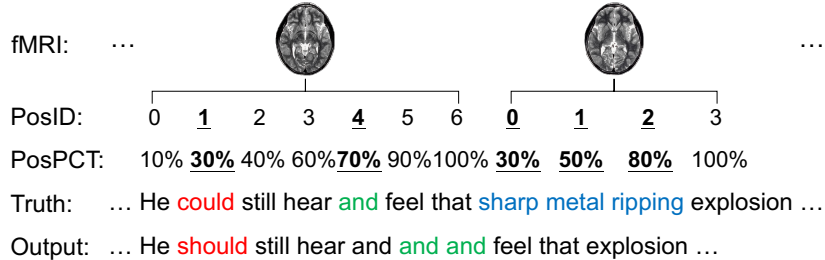


Figure 5: An example of the experiment for decoding error analysis. PosID and PosPCT stand for the word position index of truth and the percentage of index respectively.

of human is about three words per second. If pauses between sentences are excluded, the word rate within one sentence will increase to five per second. This feature of fMRI leads to the information loss problem in fMRI-to-text decoding: While brain responses of the first few heard words are recorded in one fMRI frame, information of the last heard words is lost due to the low temporal resolution, making decoding these words difficult. The latency of BOLD signal complicates the theoretical explanation of this phenomenon. But based on experimental results and previous study [18] which indicates the latency of fMRI response is about six seconds, exactly an integer multiple of repetition time (1.5s or 2s), the hypothesis of information loss is reasonable.

From sub-figure (a), (b), (c) in Figure 6, we surprisingly find PREDFT successfully reduces the error probability of the last few decoded words compared to UniCoRN. This implies the predictive coding information in brain could be utilized to alleviate the information loss, and such alleviation of information loss is closely related to the decoding accuracy. To better illustrate the degree of information loss, we propose a novel index *information loss slope* φ measuring the growth rate of error probability from the first half of decoded content to the last half,

$$\varphi = \frac{\sum_{i=6}^{10} p_i - \sum_{i=1}^5 p_i}{0.5}, \quad (7)$$

where p_i stands for the error probability of $i\%$ position. φ is expected to be around zero, as the error probabilities of different positions are supposed to be the same without information loss. However, the φ values of all compared models are high, indicating that all models suffer from information loss. PREDFT successfully mitigates information loss to some extent. As shown in sub-figure (d), (e), (f) of Figure 6, the φ score of PREDFT is lower than compared models on all the three experiments with different fMRI sequence lengths.

C Ablation Study

Three aspects of ablation experiments are conducted to analyze PREDFT. First we test whether the side network for brain prediction really improves decoding accuracy. The model PREDFT without side network (PREDFT w/o SideNet) is built with the same settings as PREDFT during training except for only keeping the main decoding network (the cross-attention layers in main decoding network are removed). The results of this model’s decoding performance are listed in Table 2, same as not using ROIs in side network (“None” in the table). The performance of PREDFT w/o SideNet is significantly worse than PREDFT in all the three experiments with different fMRI sequence length. It also performs worse than UniCoRN under most cases, which might be attributed to the pretrained language model used in UniCoRN.

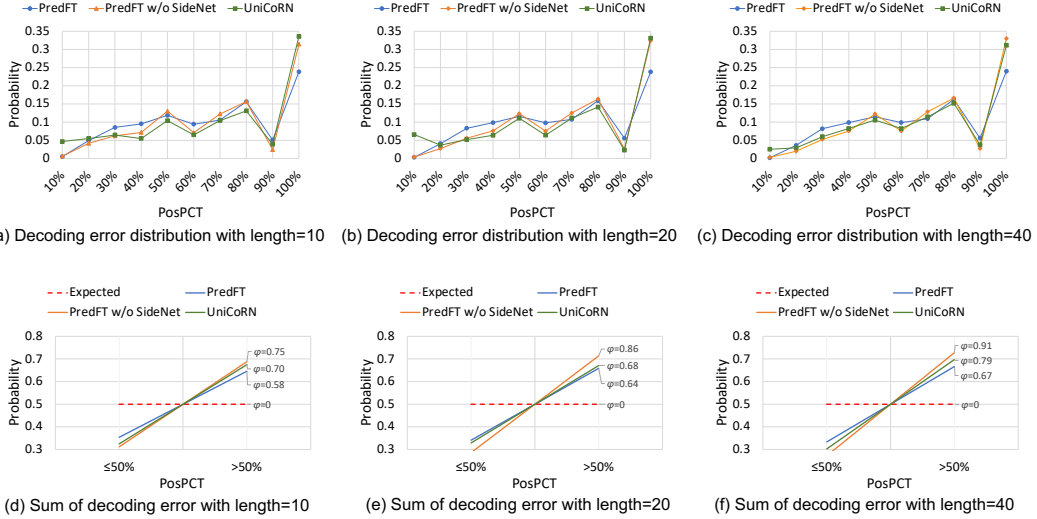


Figure 6: Information loss of different models under different fMRI sequence lengths.

Table 4: Decoding performance of PREDFT under different hyper-parameter λ .

Length	λ	BLEU-N (%)				ROUGE-1 (%)		
		$N = 1$	$N = 2$	$N = 3$	$N = 4$	R	P	F
10	1	24.73	8.39	3.92	1.86	14.07	35.28	19.53
	0.75	22.32	4.44	0.87	0.12	16.57	19.77	17.96
	0.5	22.56	4.59	1.26	0.41	15.84	19.54	17.44
	0.25	21.13	5.21	1.26	0.35	14.00	26.67	18.25
20	1	18.33	5.00	1.37	0.48	15.60	31.97	20.90
	0.75	21.15	4.71	1.22	0.44	20.58	27.13	23.35
	0.5	25.98	5.61	1.36	0.21	19.61	25.43	22.09
	0.25	25.21	5.59	1.35	0.24	20.46	26.24	22.95
40	1	20.56	5.20	1.24	0.26	21.92	28.74	24.82
	0.75	26.73	7.13	1.55	0.49	19.21	31.17	23.72
	0.5	27.80	8.29	2.00	0.54	19.53	38.95	25.96
	0.25	20.28	4.73	0.84	0.21	22.12	28.40	24.82

Besides, the decoding error distribution of PREDFT w/o SideNet is counted to verify whether the side network helps alleviate information loss. As shown in Figure 6, the error distribution of PREDFT w/o SideNet across different positions is similar to that of UniCoRN. The probability of decoding error increases as the word position moves backward within one fMRI frame, peaking at the position of the last word. PREDFT w/o SideNet severely suffers from information loss as shown in sub-figure (d), (e), (f) of Figure 6, with the highest information loss slope. The ablation experiments provide solid evidence on the effectiveness of the side network in PREDFT.

We also test the influence of hyper-parameter λ to decoding performance of PREDFT. As shown in Table 4, four different λ values ranging from 0.25 to 1 are tested in experiments with different fMRI sequence length. Empirically, PREDFT achieves relatively good decoding accuracy with $\lambda = 0.5$ in all experiments. For sequence length of 10, PREDFT performs best when λ is set as 1.